

Asymptotic Convergence of the Angular Discretization Error in the Scalar Flux Solution of the Discrete Ordinates Transport Equation with Isotropic Scattering in Two-Dimensional Cartesian Geometry

Xiaoyu Hu, Yousry Y. Azmy

Department of Nuclear Engineering, North Carolina State University, P.O. Box 7909, Raleigh, NC, USA
xhu10@ncsu.edu, yyazmy@ncsu.edu

Abstract - A two-dimensional problem with homogeneous, isotropically scattering medium in Cartesian geometry is utilized to examine angular discretization errors and verify asymptotic convergence of the numerical solution to the discrete ordinates approximation of the radiation transport equation. We use Madsen's Theorem to derive expressions for the error in the uncollided and fully collided scalar fluxes and establish upper bounds. Five quadrature types with increasing orders are utilized to evaluate the scattering source and the scalar flux. They are Level Symmetric (LS), Legendre-Chebyshev Quadrangular (LCQ), Legendre-Chebyshev Triangular (LCT), Quadruple Range (QR) and Quadruple Range S-type (QRS) quadrature sets. The Arbitrarily High Order Transport method of the Nodal type and 0-th spatial expansion order (AHOT-N0) code is employed to compute the region-averaged scalar fluxes. The results show that, in the source region, the uncollided scalar flux obtained by using LS, LCQ and LCT converges asymptotically with different rates, and such flux obtained by using QR and QRS converges faster with increasing number of angles. The convergence order of the fully collided scalar flux is greater for LCQ and LCT compared to that of the uncollided flux. However, the reason why QR and QRS quadrature sets exhibit faster than power-law convergence for the scalar flux remains to be explained. In the source-free regions, the ray-effects will be more significant and the solution error is more complicated since the uncollided angular flux is no longer exact in these regions and comprises particles leaked from the source region. It is more difficult to see the asymptotic convergence in these regions for all the quadrature types. Although the errors obtained by the LCT sets seem the largest for most cases (not considering LS because it is limited to S_{20}), they are more stable with increasing number of directions in all the cases. However, the solution calculated by the QR and QRS quadrature sets have smallest errors among all the results.

I. INTRODUCTION

Discretization methods are used in numerically solving the steady-state one-speed particle transport equation that involves both angular and spatial discretization that introduce errors into the solution. Significant efforts have been made in estimating spatial discretization errors [1–4]. Researchers began to investigate the errors due to angular discretization and developed various angular quadrature types [5–9] in order to reduce the errors in the numerical solutions.

Madsen had established an upper bound on the angular flux error due to the Discrete Ordinates approximation (S_N) [10]. In this work, we extended Madsen's theorem by developing and establishing an upper bound on the error in the scalar flux. We note that the scalar flux errors include 3 components:

1. The spatial discretization error;
2. The quadrature truncation error in computing the scalar flux from the angular flux;
3. The combined quadrature error in the scattering source and the scalar flux.

We also derived and estimated the quadrature error based on our previous work [11] and we employed a simple two-dimensional problem with a homogeneous, isotropically scattering medium in Cartesian geometry to examine these errors and verify asymptotic convergence of the numerical solution

to a reasonable limit. Five quadrature types with increasing orders are utilized to evaluate the scattering source and the scalar flux. They are Level Symmetric (LS) [12], Legendre-Chebyshev Quadrangular (LCQ) [9], Legendre-Chebyshev Triangular (LCT) [9], Quadruple Range (QR) [7] and Quadruple Range S-type (QRS) [8] quadrature sets. The LS quadrature sets require the ordinates to be rotationally symmetric about all three axes, but the angular weights become negative for quadrature orders $N > 20$, which prohibits the application for more discrete angles. The other quadrature types have reflective symmetry only, but can be expanded to any arbitrary order without negative weights. The QR and QRS quadratures accurately integrate functions that are discontinuous across octants.

In the curvilinear coordinates system, the streaming operator in the transport equation has a derivative with respect to direction, which makes the analysis more difficult. Hence, this work focuses on Cartesian coordinates only.

The paper is organized as follows. In Sec. II the quadrature error and the uncollided and the fully collided scalar flux error expressions are derived. The upper bounds on those errors are also derived based on Madsen's Theorem. A two-dimensional problem with homogeneous, isotropically scattering medium in Cartesian geometry is utilized to examine angular discretization errors and verify asymptotic convergence of the numerical solution to the discrete ordinates approximation of the radiation transport equation. The test results are demonstrated and discussed in Sec. III. In Sec. IV we summarize the

work and draw conclusions.

II. THEORY

Consider the exact steady-state one-speed transport equation with isotropic scattering and with an isotropic distributed fixed source:

$$L\psi(\mathbf{r}, \boldsymbol{\Omega}) = \Sigma_s(\mathbf{r}) \int_{4\pi} \psi(\mathbf{r}, \boldsymbol{\Omega}') d\boldsymbol{\Omega}' + S(\mathbf{r}) \quad (1a)$$

where we used standard notation and $L = \boldsymbol{\Omega} \cdot \nabla + \Sigma_t(\mathbf{r})$ is the streaming plus collision operator in $\mathbf{r} \in D$, a rectangular domain and $\boldsymbol{\Omega} \in 4\pi$, with vacuum boundary conditions

$$\psi(\mathbf{r}, \boldsymbol{\Omega}) = 0, \quad \mathbf{r} \in \partial D, \quad \boldsymbol{\Omega} \cdot \mathbf{n} < 0. \quad (1b)$$

The corresponding S_N based transport equation is

$$L_m \psi_m(\mathbf{r}) = \Sigma_s(\mathbf{r}) \sum_{n=1}^M w_n \psi_n(\mathbf{r}) + S(\mathbf{r}), \quad m = 1, 2, \dots, M \quad (2a)$$

with vacuum boundary conditions

$$\psi_m(\mathbf{r}) = 0, \quad \mathbf{r} \in \partial D, \quad \boldsymbol{\Omega}_m \cdot \mathbf{n} < 0. \quad (2b)$$

Let $\varepsilon_m(\mathbf{r}) \equiv \psi(\mathbf{r}, \boldsymbol{\Omega}_m) - \psi_m(\mathbf{r})$, $m = 1, 2, \dots, M$ be the angular flux error, where $\psi(\mathbf{r}, \boldsymbol{\Omega}_m)$ is the exact solution at direction $\boldsymbol{\Omega}_m$, and

$$\eta_M(\mathbf{r}) \equiv \int_{4\pi} \psi(\mathbf{r}, \boldsymbol{\Omega}') d\boldsymbol{\Omega}' - \sum_{n=1}^M w_n \psi(\mathbf{r}, \boldsymbol{\Omega}_n) \quad (3)$$

be the quadrature truncation error, then we have

$$L_m \varepsilon_m(\mathbf{r}) = \Sigma_s(\mathbf{r}) \eta_M(\mathbf{r}) + \Sigma_s(\mathbf{r}) \sum_{n=1}^M w_n \varepsilon_n(\mathbf{r}) \quad (4)$$

Let $T_m = \boldsymbol{\Omega}_m \cdot \nabla + \Sigma_t(\mathbf{r}) - \Sigma_s(\mathbf{r}) \sum_{n=1}^M w_n$, $m = 1, 2, \dots, M$, then Eq. (4) can be written as

$$T_m \varepsilon_m(\mathbf{r}) = \Sigma_s(\mathbf{r}) \eta_M(\mathbf{r}) \quad (5)$$

In order to explain the error components more clearly, we separate the flux into uncollided and fully collided fluxes, and use the superscripts u and c in each quantity to represent the uncollided and fully collided contributions to that quantity, respectively.

1. Uncollided Flux Errors

The error in the uncollided angular flux is obtained by setting $\Sigma_s(\mathbf{r}) = 0$ in Eq. (5):

$$T_m \varepsilon_m^u(\mathbf{r}) = 0, \quad m = 1, 2, \dots, M \quad (6)$$

Since T_m is non-singular as proved by Vladimirov [13], $\varepsilon_m^u(\mathbf{r}) = 0$, $m = 1, 2, \dots, M$, which means that the uncollided angular flux obtained by Eq. (2) is exact since the uncollided

source, comprised entirely of the fixed distributed source, is known exactly. Note that, in practice, there will be some error in $\psi_m^u(\mathbf{r})$ due to spatial discretization, but here, consistent with Ref. [10], we assume exact spatial solution. In the numerical tests presented below we utilize a reference solution obtained by Richardson extrapolation in the spatial discretization and consider the spatial discretization error in $\psi_m^u(\mathbf{r})$ negligible.

The exact uncollided scalar flux is given by

$$\phi^u(\mathbf{r}) = \int_{4\pi} \psi^u(\mathbf{r}, \boldsymbol{\Omega}') d\boldsymbol{\Omega}' \quad (7)$$

The S_N based uncollided scalar flux is

$$\phi_M^u(\mathbf{r}) = \sum_{n=1}^M w_n \psi_n^u(\mathbf{r}) \quad (8)$$

Let $E_{Q,M}^u(\mathbf{r}) \equiv \phi^u(\mathbf{r}) - \phi_M^u(\mathbf{r})$ be the angular discretization error of the uncollided scalar flux, where Q denotes the quadrature type employed in Eq. (8), thus

$$E_{Q,M}^u(\mathbf{r}) = \int_{4\pi} \psi^u(\mathbf{r}, \boldsymbol{\Omega}') d\boldsymbol{\Omega}' - \sum_{n=1}^M w_n \psi_n^u(\mathbf{r}) = \eta_M^u(\mathbf{r}) \quad (9)$$

2. Fully Collided Flux Errors

For the fully collided angular flux, the exact transport equation is

$$L_m \psi^c(\mathbf{r}, \boldsymbol{\Omega}_m) - \Sigma_s(\mathbf{r}) \int_{4\pi} \psi^c(\mathbf{r}, \boldsymbol{\Omega}') d\boldsymbol{\Omega}' = S^u(\mathbf{r}), \quad m = 1, 2, \dots, M \quad (10)$$

with vacuum boundary conditions as Eq. (1b), where the first collision source is given by:

$$S^u(\mathbf{r}) = \Sigma_s(\mathbf{r}) \int_{4\pi} \psi^u(\mathbf{r}, \boldsymbol{\Omega}') d\boldsymbol{\Omega}' \quad (11)$$

Note that $\psi^u(\mathbf{r}, \boldsymbol{\Omega}_m) = \psi_m^u(\mathbf{r})$, so the S_N based transport equation can be written as

$$T_m \psi_m^c(\mathbf{r}) = S^u(\mathbf{r}) - \Sigma_s(\mathbf{r}) \eta_M^u(\mathbf{r}), \quad m = 1, 2, \dots, M \quad (12)$$

with vacuum boundary condition as Eq. (2b). Then, the fully collided angular flux error $\varepsilon_m^c(\mathbf{r})$ satisfies

$$T_m \varepsilon_m^c(\mathbf{r}) = \Sigma_s(\mathbf{r}) [\eta_M^u(\mathbf{r}) + \eta_M^c(\mathbf{r})], \quad m = 1, 2, \dots, M \quad (13)$$

The angular flux error in Madsen's theorem satisfies

$$T_m \varepsilon_m(\mathbf{r}) = \Sigma_s(\mathbf{r}) \eta_M(\mathbf{r}), \quad m = 1, 2, \dots, M \quad (14)$$

Equation (13) has a similar form to Eq. (14), and if

1. $\Sigma_t(\mathbf{r})$, $\Sigma_s(\mathbf{r})$ are piecewise continuous;
2. $\Sigma_a(\mathbf{r}) = \Sigma_t(\mathbf{r}) - \Sigma_s(\mathbf{r}) \geq \Sigma_0 > 0$ for all \mathbf{r} ;
3. $\Sigma_s(\mathbf{r}) \geq 0$ for all \mathbf{r}

we have

$$\|\boldsymbol{\varepsilon}^c\| \leq \frac{1}{\Sigma_0} \|\boldsymbol{\eta}_M\| \quad (15)$$

where the norm is defined by

$$\|\boldsymbol{\varepsilon}^c\| \equiv \max_{1 \leq m \leq M} \sup_{\mathbf{r} \in D} |\varepsilon_m^c(\mathbf{r})| \quad (16)$$

$$\|\boldsymbol{\eta}_M\| \equiv \sup_{\mathbf{r} \in D} |\Sigma_s(\mathbf{r})(\eta_M^u(\mathbf{r}) + \eta_M^c(\mathbf{r}))| \quad (17)$$

The exact and S_N fully collided scalar flux are respectively

$$\phi^c(\mathbf{r}) = \int_{4\pi} \psi^c(\mathbf{r}, \boldsymbol{\Omega}') d\boldsymbol{\Omega}' \quad (18)$$

$$\phi_M^c(\mathbf{r}) = \sum_{n=1}^M w_n \psi_n^c(\mathbf{r}) \quad (19)$$

Let $E_{Q,M}^c(\mathbf{r}) \equiv \phi^c(\mathbf{r}) - \phi_M^c(\mathbf{r})$ be the error of the fully collided scalar flux, thus

$$E_{Q,M}^c(\mathbf{r}) = \eta_M^c(\mathbf{r}) + \sum_{n=1}^M w_n \varepsilon_n^c(\mathbf{r}) \quad (20)$$

Hence the fully collided scalar flux error is bounded by

$$|E_{Q,M}^c(\mathbf{r})| \leq |\eta_M^c(\mathbf{r})| + \sum_{n=1}^M w_n |\varepsilon_n^c(\mathbf{r})| \leq |\eta_M^c(\mathbf{r})| + \max_{1 \leq n \leq M} |\varepsilon_n^c(\mathbf{r})| \quad (21)$$

and applying the ∞ -norm to Eq.(21) we have

$$\sup_{\mathbf{r} \in D} |E_{Q,M}^c(\mathbf{r})| \leq \sup_{\mathbf{r} \in D} |\eta_M^c(\mathbf{r})| + \sup_{\mathbf{r} \in D} \max_{1 \leq n \leq M} |\varepsilon_n^c(\mathbf{r})| \quad (22)$$

Note that the last term in Eq.(22) is equivalent to $\|\boldsymbol{\varepsilon}^c\|$ which is bounded by Eq.(15), thus the fully collided scalar flux error is bounded by

$$\|E_{Q,M}^c\| \leq \|\eta_M^c\| + \frac{1}{\Sigma_0} \|\boldsymbol{\eta}_M\| \quad (23)$$

where: $\|\eta_M^c\| = \sup_{\mathbf{r} \in D} |\eta_M^c(\mathbf{r})|$.

The spatial discretization error can be omitted by taking the reference values obtained by Richardson extrapolation. The quadrature truncation error can be quantified with the uncollided scalar flux as indicated by Eq. (9) since the uncollided angular flux is exact. The combined quadrature error in the scattering source and the scalar flux is quantified with the fully collided scalar flux.

3. Quadrature Error

We expand the angular flux in Eq. (3) in Taylor series at $\mu = 0, \eta = 0$, where: $\mu = \cos \phi \sin \theta, \eta = \sin \phi \sin \theta$:

$$\begin{aligned} \eta_M(\mathbf{r}) &= \int_{4\pi} \sum_{i=0}^{\infty} \sum_{k=0}^{\infty} \frac{D^{i,k} \psi(\mathbf{r}, \boldsymbol{\Omega}')|_{00}}{i!k!} \mu^i \eta^k d\boldsymbol{\Omega}' \\ &\quad - \sum_{n=1}^M w_n \sum_{i=0}^{\infty} \sum_{k=0}^{\infty} \frac{D^{i,k} \psi(\mathbf{r}, \boldsymbol{\Omega})|_{00}}{i!k!} \mu_n^i \eta_n^k \end{aligned} \quad (24)$$

where:

$$D^{i,k} \psi(\mathbf{r}, \boldsymbol{\Omega})|_{00} = \left. \frac{\partial^{i+k} \psi(\mathbf{r}, \boldsymbol{\Omega})}{\partial \mu^i \partial \eta^k} \right|_{00} \quad (25)$$

then Eq. (24) can be rearranged as

$$\eta_M(\mathbf{r}) = \sum_{i=0}^{\infty} \sum_{k=0}^{\infty} \frac{D^{i,k} \psi(\mathbf{r}, \boldsymbol{\Omega})|_{00}}{i!k!} \delta_M^{i,k} \quad (26)$$

where:

$$\delta_M^{i,k} \equiv \int_{4\pi} \mu^i \eta^k d\boldsymbol{\Omega} - \sum_{n=1}^M w_n \mu_n^i \eta_n^k \quad (27)$$

is the quadrature truncation error of the i, k power of the angle cosines. The integral in Eq. (27) can be expressed analytically in terms of the Gamma Functions as derived in Ref. [11]. Also, $\delta_M^{i,k}$ is zero for odd i or k due to the typical reflective symmetry of the standard angular quadrature [11].

Now consider the discontinuity of the angular flux in the angular domain, say on a boundary cell with vacuum boundary conditions. Let's define the following notations:

$$\delta_{M,++}^{i,k} = \int_{\Omega^{++}} \mu^i \eta^k d\boldsymbol{\Omega} - \sum_{n=1}^M w_n \mu_n^i \eta_n^k \quad (28a)$$

$$\delta_{M,+}^{i,k} = \int_{\Omega^{+-}} \mu^i \eta^k d\boldsymbol{\Omega} - \sum_{n=1}^M w_n \mu_n^i \eta_n^k \quad (28b)$$

$$\delta_{M,-}^{i,k} = \int_{\Omega^{-+}} \mu^i \eta^k d\boldsymbol{\Omega} - \sum_{n=1}^M w_n \mu_n^i \eta_n^k \quad (28c)$$

$$\delta_{M,--}^{i,k} = \int_{\Omega^{--}} \mu^i \eta^k d\boldsymbol{\Omega} - \sum_{n=1}^M w_n \mu_n^i \eta_n^k \quad (28d)$$

where: $\Omega^{++} = \{\mu > 0, \eta > 0\}$, $\Omega^{+-} = \{\mu > 0, \eta < 0\}$, $\Omega^{-+} = \{\mu < 0, \eta > 0\}$, $\Omega^{--} = \{\mu < 0, \eta < 0\}$ and

$$D^{i,k} \psi(\mathbf{r})_{00}^{++} = \left. \frac{\partial^{i+k} \psi(\mu, \eta)}{\partial \mu^i \partial \eta^k} \right|_{0+0+}, \text{ for } \mu, \eta \in \Omega^{++} \quad (28e)$$

$$D^{i,k} \psi(\mathbf{r})_{00}^{+-} = \left. \frac{\partial^{i+k} \psi(\mu, \eta)}{\partial \mu^i \partial \eta^k} \right|_{0+0-}, \text{ for } \mu, \eta \in \Omega^{+-} \quad (28f)$$

$$D^{i,k} \psi(\mathbf{r})_{00}^{-+} = \left. \frac{\partial^{i+k} \psi(\mu, \eta)}{\partial \mu^i \partial \eta^k} \right|_{0-0+}, \text{ for } \mu, \eta \in \Omega^{-+} \quad (28g)$$

$$D^{i,k} \psi(\mathbf{r})_{00}^{--} = \left. \frac{\partial^{i+k} \psi(\mu, \eta)}{\partial \mu^i \partial \eta^k} \right|_{0-0-}, \text{ for } \mu, \eta \in \Omega^{--} \quad (28h)$$

Then, Eq. (26) can be expressed as

$$\eta_M(\mathbf{r}) = \sum_{i=0}^{\infty} \sum_{k=0}^{\infty} \frac{1}{i!k!} \sum_j D^{i,k} \psi(\mathbf{r})_{00}^j \delta_{M,j}^{i,k} \quad (29)$$

and the quadrature truncation error is

$$\delta_M^{i,k} = \sum_j \delta_{M,j}^{i,k} \quad (30)$$

where: $j = (++, +-, -+, --)$ and $\delta_{M,j}^{i,k}$ is the quadrature truncation error in each octant as determined by Ω^j .

Different quadrature types have different values of $\delta_{M,j}^{i,k}$ depending on the requirements imposed when generating the quadrature sets. The LS sets are required to conserve the even moments over the $[-1, 1]$ interval in both μ and η [12]:

$$\sum_{n=1}^M w_n \mu_n^{2m} = \frac{1}{2} \int_{-1}^1 \mu^{2m} d\mu = \int_0^1 \mu^{2m} d\mu = \frac{1}{2m+1} \quad (31)$$

for $m = 0, 1, 2, \dots, N/2$, here N is the quadrature order. Equation (31) indicates that LS sets can accurately integrate even moments in each angular quadrant Ω^j . The numerical results show that LS sets cannot integrate odd moments exactly over each individual angular quadrant Ω^j even though LS can exactly integrate odd moments over the entire unit sphere due to symmetry. Similarly, the LCQ and LCT sets can only exactly integrate the even moments in each angular quadrant Ω^j , which means that even though $\delta_M^{i,k} = 0$, we cannot conclude that $\delta_{M,j}^{i,k} = 0$ for all j .

However, although the azimuthal quadratures of the QR and QRS sets are required to integrate both odd and even moments in each angular quadrant Ω^j , whether or not the final quadrature can integrate both odd and even moments in each angular quadrant Ω^j is determined by the smallest power that the polar quadrature and the azimuthal quadrature can integrate as indicated by Ref. [11]. For example, QR461214 (the number of azimuthal angles are 4, 6, 12, 14 from top level to bottom level) set can integrate more moments over each octant than QR1-8 (the number of azimuthal angles are 1, 2, 3, ..., and 8 from top level to bottom level) set although they both have 36 discrete angles per octant, because QR1-8 set contains 1 azimuthal angle in the top level, which leads to the lowest power that the quadrature can integrate.

Note that Taylor series depends on the true solution's regularity. For a discontinuous solution, we need to consider the solution's regularity in each individual octant and combine them together.

III. RESULTS AND ANALYSIS

In this work, the cell-wise uncollided and fully collided scalar fluxes are computed by the Arbitrarily High Order Transport method of the Nodal type and 0-th spatial expansion order (AHOT-N0) code [14], and the region-averaged scalar flux errors are examined in lieu of the cell-wise values considered above.

1. Problem Configuration

The simple test problem configuration depicted in Figure 1 comprises a homogeneous-material square region, $a = b = 1$ cm, with vacuum boundary conditions on the top and right edges and reflective boundary conditions on the bottom and

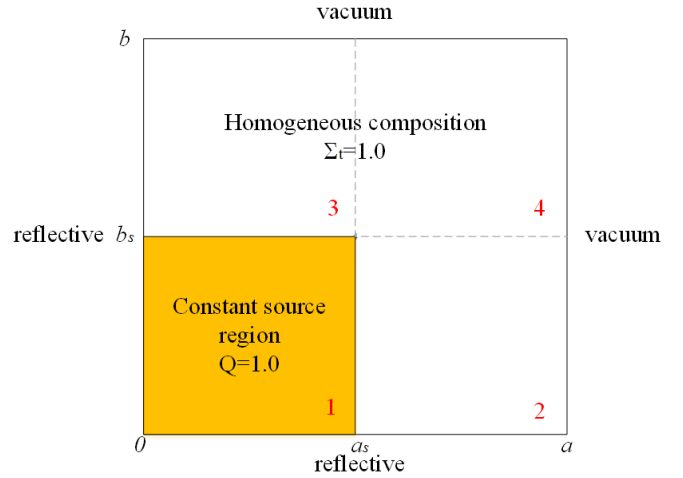


Fig. 1. Test Problem Configuration.

left edges, and a unit source only in the square region $a_s = b_s = 0.5$ cm. The cross sections in all four regions are constant, and the scattering ratio is set to 0.1.

The LS, LCQ, LCT, QR that were reviewed in Ref. [11] and QRS [8] quadrature sets with different orders are tested. The LS, LCT and QRS quadrature sets with order N have $M = N(N+2)/8$ angles per octant. The LCQ quadrature set with order N has $M = N^2/4$ angles per octant. The QR quadrature sets with order N are characterized by N polar angles and 1 to $2N-1$ azimuthal angles in each level per octant.

2. Spatial and Angular Convergence

We discretize the problem domain into $2^j \times 2^j$, $j = 1, 2, \dots, 9$ uniform spatial cells and utilize LS, LCQ, LCT, QR and QRS quadrature sets with increasing orders to examine the spatial convergence of the numerical solutions for each quadrature type, Q , and order N . The region-averaged scalar flux error is computed by first using the Richardson extrapolation to generate the spatially converged reference values, and then computing the absolute errors [15]. We observed second order convergence in the source region (Region 1) as reported in Ref. [11, 15], which establishes the spatial convergence of the region-averaged scalar flux with mesh refinement. We also observed second order convergence in Region 2 and 4 except for the uncollided scalar flux in Region 4 for all the quadrature types.

Richardson Extrapolation is used to generate the reference solution for each quadrature type separately in both spatial and angular discretization. In this work, we first carried out the spatial extrapolation to obtain the spatially reference solution and then carried out the angular extrapolation to obtain the reference solution, as indicated by the solid black line in Figure 2. We also exercised the extrapolation direction indicated by the dashed black line, obtaining reference solutions that are practically identical. However, we have not tried to accelerate along the diagonal (red line) in the discretization space.

Table I lists the reference solutions obtained by Richardson Extrapolation in both spatial and angular space for all

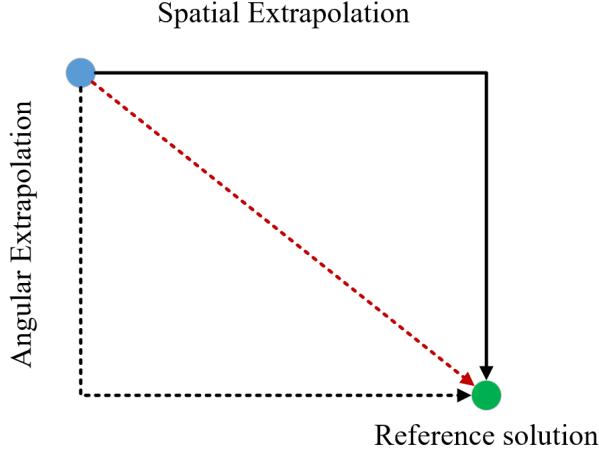


Fig. 2. Extrapolation Direction in the Discretization Space.

the quadrature types. The results show that all the solutions converge to slightly different limits for different quadrature types due to different asymptotic regimes, which means that, although the quadrature truncation goes to zero as the number of discrete angles goes to infinity [10], the convergence rate may be different among the different quadrature types, and thus the extrapolation based on some finite points may lead to different limits. The solutions obtained by LS sets are in large error due to the limited number of discrete directions.

3. Scalar Flux Errors in the Source Region

Figure 3 shows the errors of the uncollided scalar fluxes obtained by various types of quadrature sets with increasing orders against increasing number of discrete angles per octant. The reference solutions in angular discretization used in computing the plotted errors are also generated by Richardson extrapolation for each quadrature type using three sets whose orders are higher than the highest indicated order in Figure 3. Note that since the angular refinement is not uniform over the unit sphere, the extrapolation utilizes Newton's iteration to compute the reference value and the convergence order where $\frac{1}{M}$ is taken as angular mesh length. Since the LS quadrature sets have negative weights when the order $N > 20$, we cannot judge if it converges to a limit but the trend seems close to the LCQ and LCT quadrature types.

In the source region, the uncollided scalar flux error obtained by LCQ and LCT converge asymptotically with slightly different orders as listed in Table II, while those obtained by QR and QRS converge at faster rates as evident from Figure 3. We observed that if we increased the quadrature order from 1, 2, 3, ..., N , the convergence orders for LCQ sets with odd orders is 0.96 and 1.65 for the even orders. Thus, we treat LCQ sets with odd and even orders separately and we find that the convergence order for both odd and even sets is the same and equals 1.12. All the results in this section except Figure 4 show the errors obtained by LCQ sets with odd orders. The uncollided flux convergence orders for QR and QRS are omitted from Table II because they do not exhibit power-law convergence, an unexpected trend that still presents an open

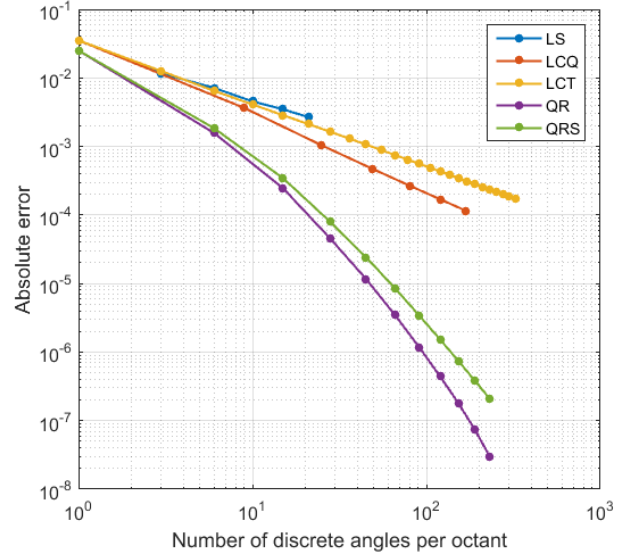


Fig. 3. Absolute Errors for Uncollided Scalar Flux in Region 1 for Different Quadrature Types.

question.

From Sec. II, we know that the uncollided scalar flux error is just the quadrature truncation error. Assuming the true angular flux has only L_j finite derivatives in Ω^j , $j = (++, +-, -+, --)$, Eq.(29) can be written as

$$\eta_M(\mathbf{r}) = \sum_j \left[\sum_{i,k=0}^{L_j-1} \frac{1}{i!k!} D^{i,k} \psi(\mathbf{r})_{00}^j \delta_{M,j}^{i,k} + R_{L_j}(\psi) \right] \quad (32)$$

where: $R_{L_j}(\psi)$ is the remainder bounded by the Remainder Estimation Theorem [16]: for all $\mu, \eta \in \Omega^j$, if $|D^{L_j} \psi_{00}| \leq \bar{\psi}_j$, then

$$|R_{L_j}(\psi)| \leq \frac{\bar{\psi}_j (|\mu| + |\eta|)^{L_j}}{L_j!} \quad (33)$$

If a quadrature set is able to integrate the polynomials $\mu^i \eta^k$ terms through maximum power P_M over each octant Ω^j and let $\bar{L} = \max_j (L_j - 1)$, $\tilde{L} = \min_j (L_j - 1)$, then we have if $P_M \geq \bar{L}$:

$$\eta_M(\mathbf{r}) = \sum_j R_{L_j}(\psi) \quad (34)$$

and if $P_M \leq \tilde{L}$:

$$\eta_M(\mathbf{r}) = \sum_j \left[\sum_{i,k=P_M+1}^{L_j-1} \frac{1}{i!k!} D^{i,k} \psi(\mathbf{r})_{00}^j \delta_{M,j}^{i,k} + R_{L_j}(\psi) \right] \quad (35)$$

otherwise, for $\tilde{L} < P_M < \bar{L}$:

$$\eta_M(\mathbf{r}) = \sum_j R_{L_j}(\psi) + \sum_{L_j-1 > P_M} \left[\sum_{i,k=P_M+1}^{L_j-1} \frac{1}{i!k!} D^{i,k} \psi(\mathbf{r})_{00}^j \delta_{M,j}^{i,k} \right] \quad (36)$$

The value of P_M depends on the quadrature types [11]. Also, the regularity(smoothness) L_j of the true solution with

	ϕ_1^μ	ϕ_1^c	ϕ_2^μ	ϕ_2^c	ϕ_4^μ	ϕ_4^c
LS	4.2762751(-1)	2.4412083(-2)	1.2246803(-1)	1.1497853(-2)	5.9712787(-2)	6.6938922(-3)
LCQ	4.2929063(-1)	2.4433447(-2)	1.2233254(-1)	1.1505697(-2)	5.9740307(-2)	6.7058623(-3)
LCT	4.2929418(-1)	2.4433270(-2)	1.2233554(-1)	1.1505985(-2)	5.9704286(-2)	6.7058651(-3)
QR	4.2929239(-1)	2.4433259(-2)	1.2233524(-1)	1.1506011(-2)	5.9707220(-2)	6.7063444(-3)
QRS	4.2929238(-1)	2.4433264(-2)	1.2233525(-1)	1.1506012(-2)	5.9706895(-2)	6.7063422(-3)

TABLE I. Reference Solutions Obtained by Richardson Extrapolation. Note: $(-x)$ means $\times 10^{-x}$.

Quadrature Type	Uncollided	Fully Collided
LCQ	1.12	~ 1.6
LCT	0.99	1.2
QR	/	~ 2.5
QRS	/	~ 2.5

TABLE II. Convergence Orders for Different Quadrature Types in Region 1.

respect to direction in each octant Ω^j is problem-specific and should not depend on the quadrature type, thus the derivative terms $D^{i,k}\psi(\mathbf{r})_{00}^j$ should not depend on the quadrature type.

Clearly from Eq.(34), the quadrature error is bounded if $P_M \geq \bar{L}$ and thus, uncollided scalar flux error is bounded. Otherwise, no matter the quadrature error is determined by Eq.(35) or Eq.(36), the value of $\delta_{M,j}^{i,k}/i!k!$ plays an important part.

Let's define $\bar{\delta}_{M,j} \equiv \max_{i,k} |\delta_{M,j}^{i,k}/i!k!|$ be the maximum quadrature truncation error. Then, we have

$$\sum_{i,k=P_M+1}^{L_j-1} \frac{1}{i!k!} D^{i,k}\psi(\mathbf{r})_{00}^j \delta_{M,j}^{i,k} \leq \left[\sum_{i,k=P_M+1}^{L_j-1} D^{i,k}\psi(\mathbf{r})_{00}^j \right] \bar{\delta}_{M,j} \quad (37)$$

Although the derivatives are difficult to evaluate, the term in the bracket of the right side of Eq.(37) is finite by definition of L_j and therefore this term is finite. Hence, the quadrature truncation error is bounded. In our case, $P_M = 0$ for all quadratures, the only difference among all the quadrature types is the maximum quadrature truncation error $\bar{\delta}_{M,j}$.

Figure 4 shows the maximum quadrature truncation error versus increasing number of discrete angles per octant. Comparing with the results in Figure 3, we observed the same trend, which indicates that the uncollided scalar flux error in the source region is bounded by Eq.(35) or Eq.(36) depending on the regularity of the solution. Meanwhile, the quadrature error also includes the summation over remainders of each octant which is a function of μ and η . We conjecture that makes it different among the results obtained by different quadrature types.

The difference in the obtained errors for the lowest order, i.e. one angle per octant, is caused by the different polar angles prescribed by LS, LCQ, and LCT on the one hand versus QR and QRS on the other hand. Due to reflective symmetry, the only azimuthal angle is 45 degree for all the quadrature types with the lowest order. The polar angle is the root of Cheybshev Polynomial for LCT and LCQ sets, and Gauss-Christoffel Polynomial for QR and QRS sets.

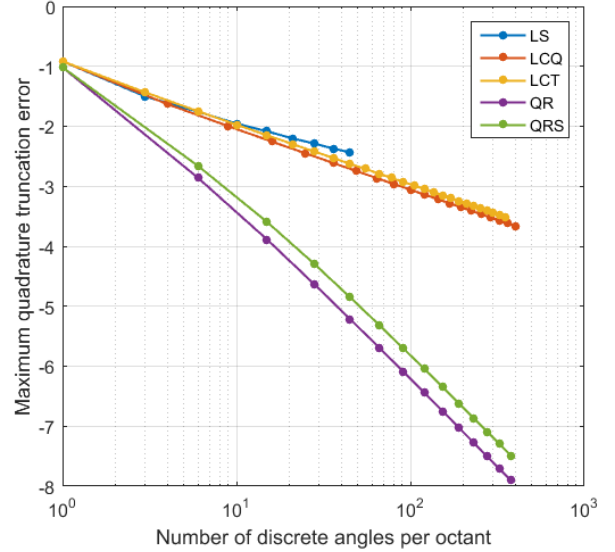


Fig. 4. Maximum quadrature error.

Figure 5 shows the absolute errors of fully collided scalar fluxes in Region 1 against increasing number of discrete angles per octant. The turning points of QR and QRS quadrature sets are due to the fact that the fluxes obtained by these two quadrature sets do not trend monotonically with increasing quadrature orders. Here too, the LCQ and LCT errors are greater than those of QR and QRS but all errors are clearly asymptotic for $M > 30$.

Note that the fully collided flux convergence orders of LCQ and LCT are greater than the corresponding uncollided flux convergence orders as indicated in Table II, which is still under investigation.

4. Scalar Flux Errors in the Source-free Regions

Figure 6 shows the absolute errors of the uncollided scalar fluxes against increasing number of discrete angles per octant in Region 2. We observed that the error curves are not as smooth as those in Region 1, especially for the QR sets because in this region, the uncollided source comprises particles leaked from the source region along discrete directions, the angular flux is not exact anymore. Thus the scalar flux error comprises not only the quadrature error. In fact, we observed the uncollided scalar fluxes obtained by the LCQ and QR sets do not increase or decrease monotonically with increasing number of discrete angles, which means that these fluxes do

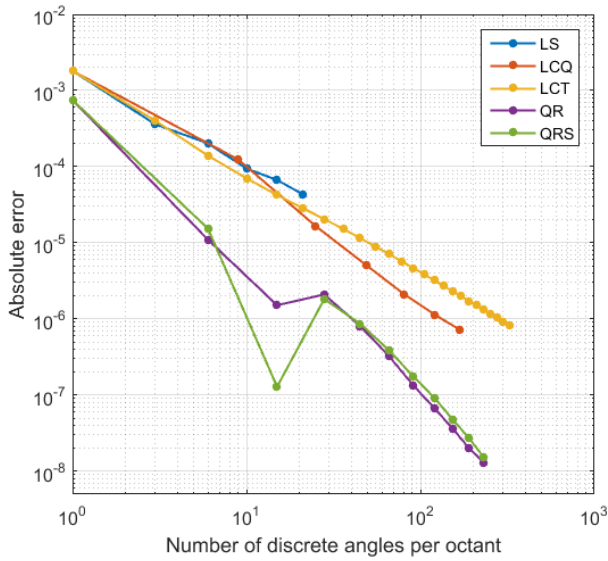


Fig. 5. Absolute Errors for Fully Collided Scalar Flux in Region 1.

not converge asymptotically. So we used the highest three points which can be extrapolated to get the reference solutions. That's why the error of LCQ seems steep and there is a turning point in the QR curve. For other quadrature types, the QR and QRS sets outperform others with smaller errors.

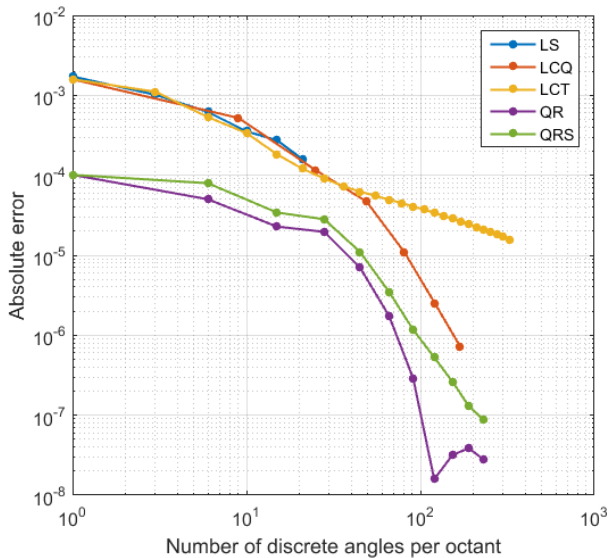


Fig. 6. Absolute Errors for Uncollided Scalar Flux in Region 2.

Figure 7 shows the absolute errors of the fully collided scalar fluxes against increasing number of discrete angles per octant in Region 2. Similarly, the error curves are not as smooth as those in Region 1. For the fully collided scalar flux error, it is more complicated since this component of the error includes the error from the source region. However, the LCQ

and LCT errors are greater than those of the QR and QRS errors. The LCQ and LCT errors seem to trend asymptotically with the number of angles with relatively close convergence orders.

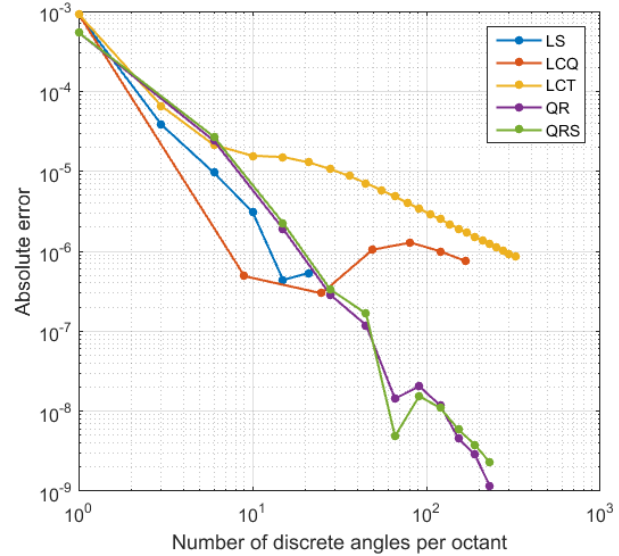


Fig. 7. Absolute Errors for Fully Collided Scalar Flux in Region 2.

In Region 4, we observed that the uncollided scalar flux obtained by all the quadrature types converges but not quadratically in the spatial variable like it does in the other regions. Figure 8 shows the absolute errors of the uncollided scalar fluxes against increasing number of discrete angles per octant in this region. Although we observed that even for the same quadrature type, the spatial convergence order is different for different quadrature orders, the flux errors of the LCT sets converges almost asymptotically with order 0.96 in the angular discretization. Again, the QR and QRS sets outperform the other quadrature types but their trends are not definitively asymptotic.

Figure 9 shows the absolute errors of the fully collided scalar fluxes against increasing number of discrete angles per octant in Region 4. From the results, we observe the lack of asymptotic convergence of the angular discretization error for all quadrature types, except potentially LCT that appears to converge faster than a power-law. We also note that the big advantage of QR and QRS in terms of smaller error than the other quadratures is far diminished in this case.

IV. CONCLUSIONS

In this paper, we have derived the uncollided and fully collided scalar flux angular-discretization error expressions and established upper bounds on these errors in the source region based on Madsen's theorem. The uncollided angular flux obtained by the S_N transport equation does not incur angular discretization error, and the uncollided scalar flux error stems from the angular quadrature truncation error only. The fully collided angular flux error is bounded by the quadrature

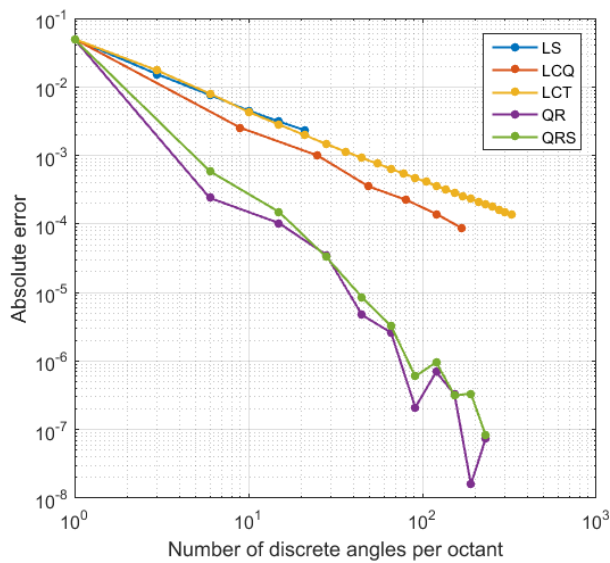


Fig. 8. Absolute Errors for Uncollided Scalar Flux in Region 4.

truncation error and the corresponding scalar flux error is also bounded by the quadrature truncation error. Also, we have derived the quadrature error considering the discontinuous angular flux at angular boundary and observed the asymptotic convergence of the quadrature maximum truncation error.

A simple test problem is solved using five quadrature types and AHOT-N0 code with spatial and angular mesh refinements. Richardson extrapolation is used to obtain the region-averaged reference values for uncollided and fully collided scalar flux with spatial and angular refinement. The results show that the uncollided scalar flux obtained by using LS, LCQ and LCT converges asymptotically with different rates, and such flux obtained by using QR and QRS converges faster with increasing number of angles. That's because of the difference among the maximum quadrature truncation error $\delta_{M,j}$ in each octant. The convergence order of the fully collided scalar flux is greater for LCQ and LCT quadrature sets compared to their respective orders for the uncollided flux.

The scalar flux error in the source-free regions (Region 2 to 4) is more complicated to analyze since the uncollided source in those regions comprises particles leaked from the source region along discrete directions. Since there is no distributed fixed source, ray-effects will be more significant in these regions. It is more difficult to see the asymptotic convergence in these regions for all the quadrature types. Although the error obtained by the LCT sets seems the largest, they are more stable with increasing number of directions in all the cases. However, the solutions calculated by the QR and QRS quadrature sets have the smallest errors among all the results for this region.

Nevertheless, the reason why QR and QRS quadrature sets exhibit faster than power-law convergence in the source region for the uncollided scalar flux remains to be explained. More efforts are needed to verify the relationship between the solution error and the quadrature error. Also the method of

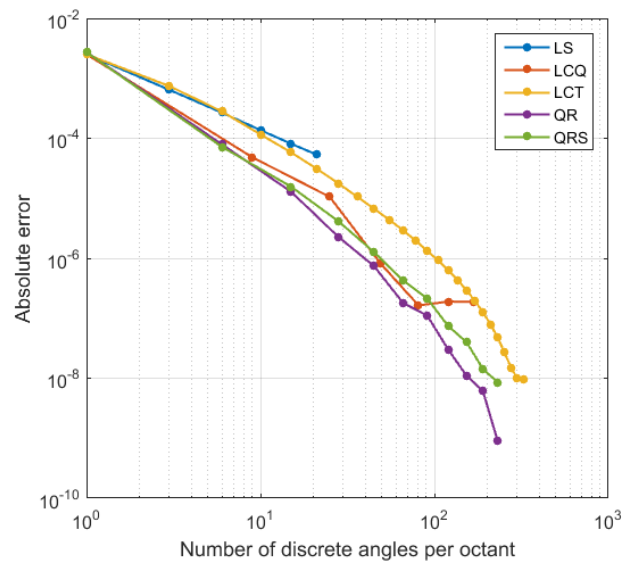


Fig. 9. Absolute Errors for Fully Collided Scalar Flux in Region 4.

extrapolation in both spatial and angular variables along the diagonal should be considered in future work.

V. ACKNOWLEDGMENTS

This material is based upon work by the second author (YYA) supported by the Department of Energy National Nuclear Security Administration under Award Number(s) DE-NA0002576.

REFERENCES

1. J. I. DUO and Y. Y. AZMY, "Spatial Convergence Study of Discrete Ordinates Methods Via the Singular Characteristic Tracking Algorithm," *Nuclear Science and Engineering*, **162**, 41 (2009).
2. E. W. LARSEN and P. NELSON, "Finite-Difference Approximations and Superconvergence for the Discrete-Ordinate Equations in Slab Geometry," *SIAM J. Numer. Anal.*, **19**, 334 (1982).
3. S. SCHUNERT and Y. Y. AZMY, "Comparison of Spatial Discretization Methods for Solving the S_n Equations Using a Three-Dimensional Method of Manufactured Solutions Benchmark Suit with Escalating Order of Nonsmoothness," *Nuclear Science and Engineering*, **180**, 1–29 (2015).
4. J. I. DUO and Y. Y. AZMY, "Error Comparison of Diamond Difference, Nodal, and Characteristic Methods for Solving Multidimensional Transport Problems with the Discrete Ordinates Approximation," *Nuclear Science and Engineering*, **156**, 139 (2007).
5. C. D. AHRENS, "Lagrange Discrete Ordinates: A New Angular Discretization for the Three-Dimensional Linear Boltzmann Equation," *Nuclear Science and Engineering*, **180**, 273–285 (2015).
6. J. J. JARRELL and M. L. ADAMS, "Discrete-Ordinates

- Quadrature Sets Based on Linear Discontinuous Finite Elements,” *Int. Conf. Math & Comp. Meth. Applied to Nuclear Sci. & Eng.* (2011).
7. I. K. ABU-SHUMAYS, “Angular Quadrature For Improved Transport Computations,” *Transport Theory and Statistical Physics*, **30**, 169–204 (2001).
 8. P. J. SPENCE, “The Generation of Arbitrary Order, Non-Classical, Gauss-Type Quadrature for Transport Applications,” *Journal of Computational Physics*, **296**, 25–27 (2015).
 9. W. F. WALTERS, “Use of the Chebyshev-Legendre Quadrature Set in Discrete-Ordinate Codes,” Tech. Rep. LA-UR-87-3621, Los Alamos Scientific Laboratory (1987).
 10. N. K. MADSEN, “Pointwise Convergence of the Three-dimensional Discrete Ordinate Method,” *SIAM J. Numer. Anal.*, **8** (1971).
 11. X. HU and Y. Y. AZMY, “Error Due to Angular Discretization in the Discrete Ordinates Approximation of the Transport Equation in Two-dimensional Cartesian Geometry,” *Proceeding of Physics of Reactors conferences (PHYSOR) 2016* (2016).
 12. K. D. LATHROP and B. G. CARLSON, “Discrete Ordinates Angular Quadrature of the Neutron Transport Equation,” Tech. Rep. LA-3186, Los Alamos Scientific Laboratory (1965).
 13. V. S. VLADIMIROV, “Mathematical Problems in The One-velocity Theory of Particle Transport,” *Trudy Mat. Inst. Steklov.*, **6**, 52–63 (1961).
 14. Y. Y. AZMY, “Arbitrarily High Order Characteristic Methods for Solving the Neutron Transport Equation,” *Annals of Nuclear Energy*, **19**, 593–606 (1992).
 15. L. B. BARICHELLO, C. B. PICOLOTO, A. TRES, and Y. Y. AZMY, “Recent Studies on the Asymptotic Convergence of the Spatial Discretization for Two-Dimensional Discrete Ordinates Solutions,” *Journal of Computational and Theoretical Transport* (2015).
 16. T. M. APOSTOL, *Calculus*, vol. 1, Wiley (1991).